Springer

KSME

Journal of Mechanical Science and Technology 32 (10) (2018) 4697~4709
www.springerlink.com/content/1738-494x(Print)/1976-3824(Online)
DOI 10.1007/s12206-018-0917-y

Effect of teeth bending and mushrooming damages on leakage performance of a labyrinth seal †

Xin Yan[1,*], Xinbo Dai[1], Kang Zhang[1], Jun Li[1] and Kun He[2]

[1]*Institute of Turbomachinery, Xi'an Jiaotong University, Xi'an 710049, China*
[2]*MOE Key Laboratory of Thermo-Fluid Science and Engineering, Xi'an Jiaotong University, Xi'an 710049, China*

(Manuscript Received February 5, 2018; Revised May 23, 2018; Accepted June 18, 2018)

Abstract

To achieve higher aerodynamic performance, turbine usually works at tight clearance, which results in inevitable rub between the rotor and stator parts of labyrinth seal due to vibrations, misalignment, mechanical force, thermal stress, etc. In the rubbing events, contact between labyrinth fin and rotor part will commonly induce the teeth bending and mushrooming damages, which significantly affect the discharge performance of a labyrinth seal. To account for the influence of teeth bending and mushrooming on leakage performance of a straight-through labyrinth seal, the leakage rates and flow fields in the worn labyrinth seal are measured and also compared with the original design cases. With numerical methods, the discharge behaviors of the labyrinth seal with different degrees of bending and mushroom damages are analyzed. It shows that the predicted leakage performance and flow fields in the labyrinth seals match well with the experimental tests. For the bending cases, the leakage rates and flow patterns in labyrinth seals are dependent on the effective clearance and bending angle. The leakage ratio of forward bending case is smaller than that of backward bending case with the same geometrical dimensions. However, for the mushroomed labyrinth seals, the leakage rates and flow patterns are much dependent on the effective clearance but slightly dependent on the mushroom radius.

Keywords: Labyrinth seal; Rub; Leakage; Bending; Mushrooming

1. Introduction

Labyrinth seal is one of the primary sealing devices in modern turbo machines (steam turbine, gas turbine, compressor, etc.) due to its simplicity, low cost and easier installation characteristics. In practice, the labyrinth seal not only significantly affects the aerodynamic performance [1], but also influences the operation safety [2] and interval of overhaul for turbine unit [3]. Therefore, many research activities have dedicated to develop advanced labyrinth seals to improve the sealing effectiveness since 1980s [1]. However, some critical problems remain in turbo machines due to the failure of labyrinth seals, especially in the transient periods of startup, shutdown and hot restart [4]. In these cases, the interference of seal rotor and stator often occurs, which leads primarily to damage the labyrinth fin (for instance, break-off, bending, mushrooming, etc.) or the opposite surface (for instance, rub groove). The damages in labyrinth seal will result in deviations of clearance gap from the original design, thus significantly affect the realistic performance (aerodynamic, heat transfer, cooling, rotordynamics, etc.) of labyrinth seal in contrast to the original design [5].

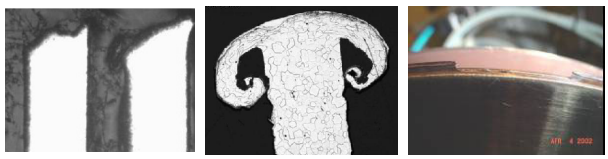

(a) Wear-off (b) Mushrooming (c) Break-off

Fig. 1. Photos of damaged labyrinth fin [4].

Fig. 1 illustrates the common damages in labyrinth fin after rub. Note the seal geometry varies a lot compared with the original design, especially near the fin tip. As pointed out in Ref. [4], wear of labyrinth fin will significantly influence the jet speed across the clearance gap. Moreover, the deformation of labyrinth fin changes the area of seal chamber which determines the dissipation of leakage jet. Therefore, the discharge behavior [6], heat transfer [7] and rotordynamic performance [8] of the worn labyrinth seal will be quite different with the original design.

For a labyrinth seal, the type of wear mainly depends on materials of labyrinth fin and its opposite part [4, 5]. Evidences have shown that, if the labyrinth fin is made from soft

*Corresponding author. Tel.: +86 29 82663195, Fax.: +86 29 82668704
E-mail address: xinyan@mail.xjtu.edu.cn
† Recommended by Associate Editor Hyoung-Bum Kim

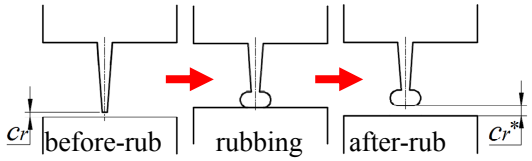

(a) Mushrooming process

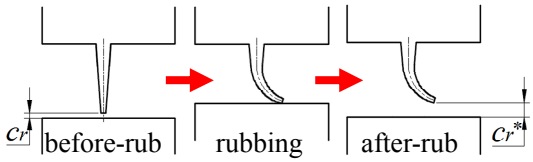

(b) Bending process

Fig. 2. Mushrooming and bending processes in labyrinth seal.

material, for example, aluminum, thermoplastic material, etc., the labyrinth fin tip is likely to be worn-off or mushroomed [4] in the rubbing events. If the labyrinth fin is made from hard metal, for example, steel, steel alloy, the bending damage is most probably occurred when seal rotor and stator contact each other [5]. Fig. 2 depicts the mushrooming and bending processes for the labyrinth seal. It is evident that the effective sealing clearance and fin geometry change a lot in the rubbing process. Therefore, a deep insight into the flow patterns and leakage rate in labyrinth seal after rub would be beneficial to the leakage control in realistic operation conditions.

Since the main function of labyrinth seal is to control leakage rate in turbo machines, most of the previous studies struggled to investigate the leakage performance of labyrinth seal. The representative experimental and numerical work carried out by Wittig et al. [9] showed that the pressure ratio and geometrical parameters (such as the clearance, pressure ratio, fin number, etc) are the main influence factors to determine leakage rates and flow patterns in labyrinth seals. Then, Schramm et al. [10] visualized the flow fields in the stepped labyrinth seal with LDV (laser Doppler velocimetry) technology, and also measured the leakage rates at a range of pressure ratios and three different sealing clearances. Their results indicated that the leakage rate in stepped labyrinth seal is nearly proportional to the sealing clearance and pressure ratio. Subsequently, Paolillo et al. [11] experimentally revealed that the leakage rate in labyrinth seal is affected by the rotor speed and inlet preswirl ratio. Micio et al. [12] found that the pressure ratio, Reynolds number and sealing clearance have significant influence on the leakage rate and flow fields in a straight-through labyrinth seal. However, these studies [9-12] mainly focused on the relations between leakage rate and influence factors, including the operation conditions and geometrical parameters, for the original design cases. Although such studies are very helpful for the labyrinth seal design, it still not well suited for the sealing performance evaluation in realistic operation process.

With such background, a few researchers turned their research interests to the rub characteristic in labyrinth seals in recent years. Whalen et al. [13] systematically analyzed the geometry deformations for a typical metallic labyrinth seal in the rubbing process. By testing the thermal properties of various materials for labyrinth seals, a thermoplastic labyrinth seal concept was presented to solve the problem of enlarged gap width when rub occurs for centrifugal compressors. Ghasripoor et al. [4] experimentally investigated the heating and melting mechanisms in labyrinth fin during rubbing process. Their study showed that the thermal conductivity and geometry are the main factors to influence the wear behavior. Xu's [5] numerical study revealed that the bending and mushrooming significantly increase the leakage rate for labyrinth seal, and also, the flow patterns vary a lot in the bent seal chamber in contrast to the original design. Based on Micio et al's experimental tests [12] and Xu's rub models [5], Yan et al. [7] investigated the effect of bending and mushrooming damages on heat transfer characteristic in a straight-through labyrinth seal. Their study showed that the bending damage has little influence on the overall Nusselt number distributions on the seal rotor and stator, while the mushrooming rub has a pronounced effect on heat transfer in the labyrinth seals in contrast to the original design. Herrmann et al. [6] carried out the finite element analysis to predict the deformation geometry for labyrinth seal in rubbing process. They found that the contact heat transfer coefficient has a pronounced effect on the deformed shape of labyrinth fin. In their study, a new concept of flexible seal was presented to mitigate the rub damage for labyrinth fin in rubbing event. Pychynski et al. [14] presented a theoretical method to investigate the thermo-mechanical performance of labyrinth seal during rub process. They found that the temperature gradient in labyrinth fin has a minor effect on stress, whereas the temperature rise plays an important role in the risk of fin crack in rubbing event. Dogu et al. [15] numerically investigated the leakage degradation for the labyrinth seal with different types of wear in labyrinth fin and stator surface. Their numerical results indicated that, for the tooth-wear, unworn, rounded and mushrooming damages affect the leakage rate from the least to greatest. Recently, as the honeycomb seal is gradually exhibiting superior performance over the conventional labyrinth seal, some studies dedicated to the wear damages in labyrinth seal with honeycomb land were presented in open publications. For example, Chougule et al. [16] numerically investigated the leakage performance of labyrinth seal with worn honeycomb. They found that the leakage rate is increased with the increase of rub groove depth in lower clearance case, but it is not varied significantly in larger clearance case. The groove width of honeycomb land is also an important influence factor for the discharge behavior of labyrinth-honeycomb seal. Collins and Teixeira [17] experimentally and numerically investigated the sealing performance degradation in the labyrinth seal with worn honeycomb. Their research showed that wear in the honeycomb cells increases the leakage rate, particularly in the case of "teeth located centrally below the rub groove". Pychynski et al. [18] measured the rub behavior between the

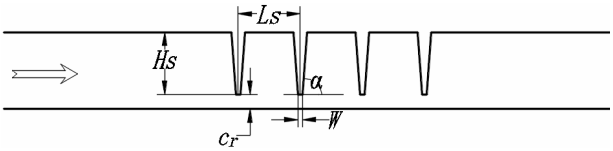

(a) Original design case

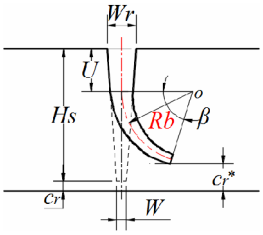

(b) Bending case

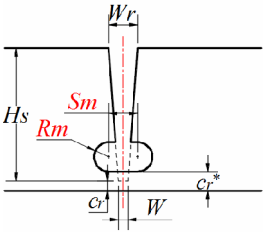

(c) Mushrooming case

Fig. 3. Geometrical parameters of the labyrinth seals.

labyrinth fin and honeycomb liner. In their study, the friction temperature field and wear performance were analyzed at a range of incursion rates and friction velocities. It showed that there is a strong interaction between contact forces, friction, temperature field, and wear behavior in the rubbing event.

In this study, leakage performance of the labyrinth seal with bending and mushrooming damages are investigated by experimental tests and CFD analysis. At first, the measurements of leakage rates and visualizations of flow fields in labyrinth seals with bending and mushrooming damages are presented and compared with the original design cases. With the experimental data, the present numerical methods are carefully validated. Then, with the numerical methods, the leakage rates and flow patterns in the labyrinth seal with different degrees of bent and mushrooming damages are computed. The effects of bending and mushrooming damages on the discharge behaviors in the labyrinth seals are analyzed and also compared with the original design cases. Notice all experiments and numeric simulations in the present study are carried out in non-rotating conditions. However, with the theories presented in Refs. [19, 20], the results can be extended to the rotating cases.

2. Numerical methods

2.1 Geometrical models

In this study, a straight-through labyrinth seal with four fins is selected as the research objective. The geometrical parameters for the original design, bending and mushrooming cases are illustrated in Fig. 3. The geometrical dimensions of the original design are listed in Table 1.

Since the bending geometries of labyrinth seals in realistic operation conditions are quite complex, in the present study Xu's bending model [5] is adopted to describe the bending damage in labyrinth fin. This bending model is based on three assumptions (see Fig. 3(b)):

(1) The centerline of bent portion is an arc with radius *Rb*.

(2) The arc of centerline is tangential to the centerline of the unbent portion.

(3) The thickness of bent portion is the same with the original design.

Table 1. Geometrical dimensions for the original design case.

Parameter	Value
Hs (mm)	16.4
Ls (mm)	16.4
c_r (mm)	1.2, 1.7, 2.2, 2.7
W (mm)	1.2
α (deg.)	86

Table 2. Geometrical dimensions for the bending cases.

Case	c_r^* (mm)	*β* (deg.)	*U* (mm)
BB1S, FB1S	2.39	76.27	9.96
BB1M, FB1M	3.50	107.58	9.96
BB1L, FB1L	4.66	174.43	9.96
BB2S, FB2S	2.39	55.96	5.27
BB2M, FB2M	3.50	74.45	5.27
BB2L, FB2L	4.66	90.22	5.27
BB3S, FB3S	2.39	44.67	0
BB3M, FB3M	3.50	59.79	0
BB3L, FB3L	4.66	72.43	0

Table 3. Geometrical dimensions for the mushrooming cases.

Case	c_r^* (mm)	*Rm* (mm)
MR1S	2.39	1.2
MR2S	2.39	1.8
MR1M	3.50	1.2
MR2M	3.50	1.8
MR1L	4.66	1.2
MR2L	4.66	1.8
MR3V	5.67	1

For the mushrooming case, the mushroomed fin tip is simplified as an arc with radius *Rm* at each side. The mushrooming model is based on two assumptions (see Fig. 3(c)):

(1) The mushroomed arcs are symmetrical about the centerline of labyrinth fin.

(2) The distance between two arc centers is two times of the mushroom radius, i.e. $Sm = 2Rm$.

Based on above assumptions, nine backward bending (BB) cases, nine forward bending (FB) cases and seven mushrooming (MR) cases are selected to investigate the effects of fin damages on leakage performance in labyrinth seal. The detailed geometrical dimensions of the bending and mushrooming cases are listed in Tables 2 and 3, respectively. In Table 2, the case numbers "1", "2" and "3" mean that the tooth unbent height *U* is large, intermediate and small, respectively. "S", "M" and "L" represent the cases with small clearance, medium clearance and large clearance, respectively. In Table 3,

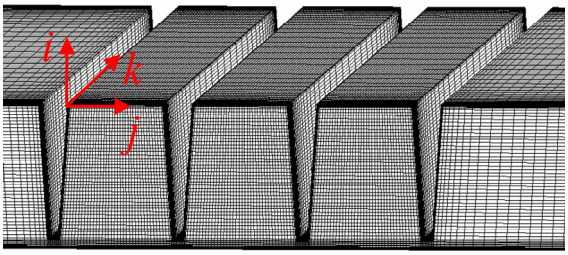

(a) Design case

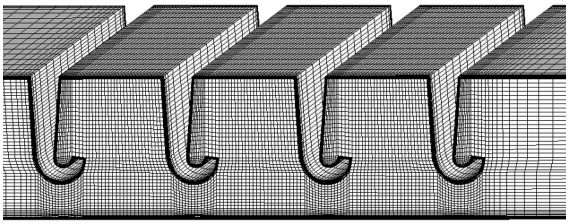

(b) Backward bending

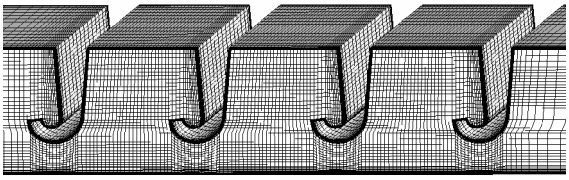

(c) Forward bending

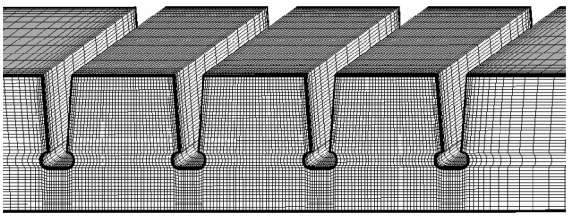

(d) Mushrooming

Fig. 4. Meshes for different models.

the case numbers "1", "2" and "3" mean different values of the mushroom radius *Rm*. "V" represents the experimental test case.

2.2 Computational meshes

In the numerical simulations, multi-block structured grids are generated with the commercial software ANSYS ICEM 11.0. Fig. 4 illustrates the meshes for labyrinth seals in original design and worn cases. For the worn cases, O-type grids are built near the wall surfaces to improve the mesh quality. In all cases, the minimum orthogonalities of the computational meshes are controlled above 30°. To capture the flow physics in boundary layers, the near wall grids are refined to resolve the gradient of flow variables. The growth factor of meshes near wall is set to 1.2, and the wall adjacent cell distance is set to be 0.001 mm, which ensures $y^+<1$ in most part of the computational domain.

Table 4 shows the grid sensitivity analysis for the original design case with three mesh densities. It indicates that the grid density has little influence on the computed leakage rate as the grid number reaches above 0.6 million. Finally, the mesh number for original design case is selected to be 1.2 million, and the mesh number for the worn case is increased to 1.7 million dues to the complex flow patterns in seal chambers.

Table 4. Computed leakage rates with different mesh densities (π = 1.5).

Grid number	Leakage rate (kg/s)	Experiment (kg/s)
600000	0.072037	0.0722
1200000	0.072039	
2420000	0.071973	

2.3 Computational methods

The commercial software ANSYS CFX 11.0 is adopted to solve the three-dimensional compressible RANS (Reynolds averaged Navier-Stokes) equations. The air ideal gas model is used to simulate the gas property in labyrinth seal. A high-resolution scheme [21] is adopted for the discretization of advection term. To solve the turbulence flow information, SST k-ω and k-ε turbulence models are used and compared with each other.

The inlet and outlet boundary conditions in labyrinth seals are set according to the experimental tests. At the seal inlet, the total pressure (depending on pressure ratio) and temperature (303.15 K) are specified. At the seal outlet, the averaged static pressure (97.5 kPa) is opposed. Since there is no heat transfer involved in the experimental tests, all wall boundaries are assumed to be adiabatic.

As the root mean square residuals of continuity equation, momentum equations, energy equation and turbulence equations reach 10^{-6}, the iterations are considered to be converged.

2.4 Definitions

The pressure ratio π is defined by

$$\pi = \frac{P_0}{P_1} \tag{1}$$

where P_0 is the inlet total pressure, and P_1 is the outlet static pressure.

The leakage ratio ξ is defined by

$$\xi = \frac{m_{worn}}{m_{design}} \tag{2}$$

where m_{worn} is the leakage rate of worn case, and m_{design} is the leakage rate of the original design case (c_r = 1.2 mm).

The Reynolds number is defined by

$$Re = \frac{\rho V d}{\mu} = \frac{m}{\mu B} \tag{3}$$

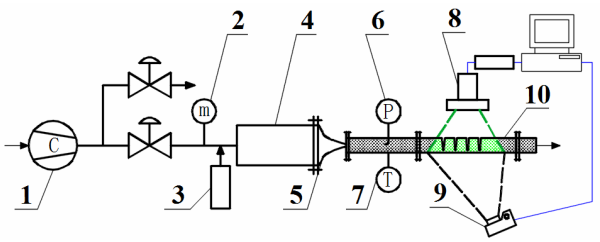

① screw compressor ② flowmeter ③ smoke generator
④ calming section ⑤ contraction section ⑥ total pressure probe
⑦ thermocouple ⑧ laser generator ⑨ PIV camera ⑩ test section

Fig. 5. Schematic diagram of the test rig.

where ρ is the fluid density. μ is the fluid dynamic viscosity. V is the characteristic velocity. d is the characteristic length. B is the width of test section.

3. Experimental setup

The experimental tests were conducted on a subsonic open loop test rig, which is located in Turbomachinery Laboratory at Xi'an Jiaotong University. It mainly consists of flowmeter, control valves, smoke generator, calming section, contraction section, test section, and PIV measurement system (CCD cameras, laser generator, etc.). Fig. 5 shows the diagrammatic sketch of the test rig. In the experimental tests, the air at atmospheric pressure and ambient temperature is pressurized by a screw compressor. The maximum pressure of the air at compressor outlet can be reached up to 0.7 MPa. A ROTORK turbine flowmeter QWLJ-080 is installed downstream the compressor to measure the mass flow rate of air. The measurement uncertainty of the flowmeter is ±1 % if the mass flow rate ranges from 0.028 kg/s to 0.14 kg/s. If the mass flow rate is less than 0.028 kg/s, the maximum measurement uncertainty will be ±2 %. Downstream the flowmeter, a smoke generator is installed to seed the flow with particles. The compressed air enters the calming section to adjust the flow in the test section. In the calming section, a turbulence grid with 0.5 mm diameter wires is installed to generate a uniform flow condition at the inlet of test section. The photograph of the test rig is illustrated in Fig. 6.

Fig. 7 shows the close-up view of test section. The test channel is 180 mm in length, 320 mm in width and 17.4 mm in height. The inlet temperature T_0 and total pressure P_0 of the leakage flow are measured with a K-type thermocouple and a total pressure probe, respectively. The static pressure in each chamber is measured with the hydrostatic probes. The uncertainties of measured temperature and pressure are about ±0.3 K and ±10 Pa, respectively. The uncertainty of piezoelectric transducer for the probe is 0.7 ‰. In this study, four different test sections are considered, which are illustrated in Fig. 8.

Particle image velocimetry (PIV) technique is used to visualize the meridian velocity fields in labyrinth seals. The PIV measurements are performed independently from the leakage rate measurements. The PIV measurement contains four steps: (1) Seeding the flow with particles, (2) illuminating the particles with a laser sheet, (3) recording two successive images with a double exposure camera synchronized to laser pulses, (4) post-processing the measured velocity fields. Fig. 9(a)

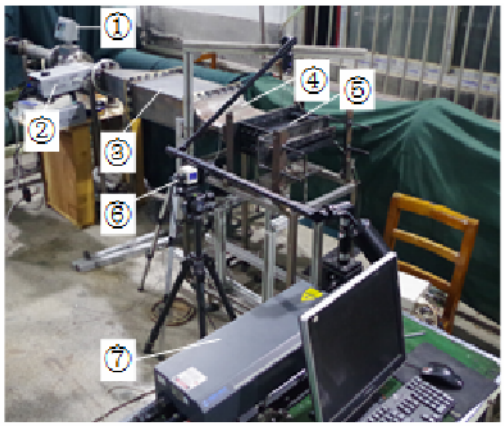

① flowmeter ② smoke generator ③ calming section
④ contraction section ⑤ test section ⑥ CCD camera
⑦ laser generator

Fig. 6. Photograph of the test rig.

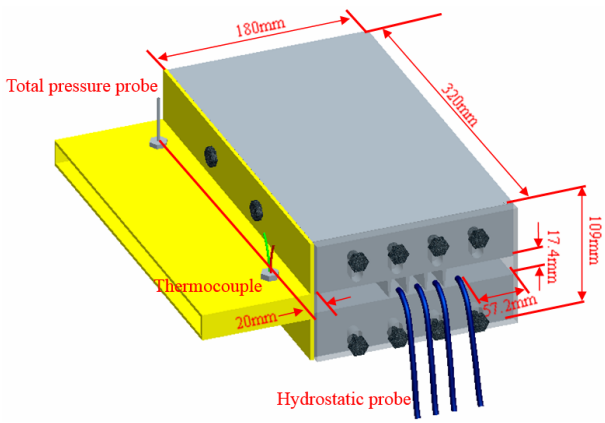

Fig. 7. Detailed view of the test section.

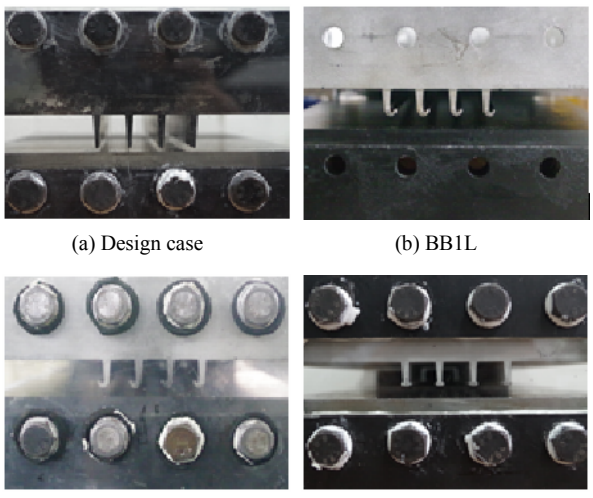

(a) Design case (b) BB1L

(c) FB1L (d) MR3V

Fig. 8. Photographs of the tested seals.

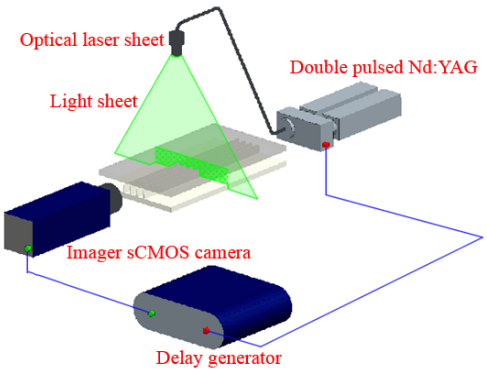

(a) PIV system

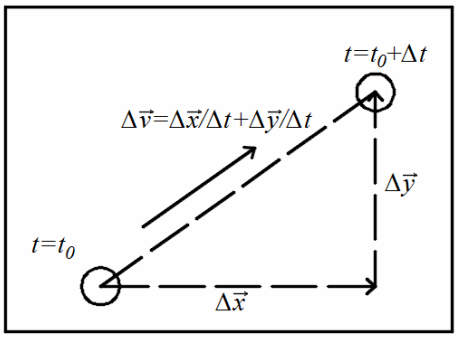

(b) Velocity vector of a particle

Fig. 9. The principle of PIV measurements.

shows PIV system in the present study. To generate liquid particles, the fog smoke liquid (DJ Power) is atomized by a smoke generator (label ③ in Fig. 5) in the seeding system. In the test section, perspex material is used as the window for PIV measurements. The perspex wall, where is not used for the laser penetration and image taken, is painted black in the visualization tests. To reduce the influence of natural light, all PIV measurements are carried out in the evenings. In the illuminating system, an Nd:YAG dual cavity pulse laser is adopted to provide two pulses with 145 mJ/pulse at 532 nm. The pulse rate is fixed at 15 Hz. In the measurement, the collinear laser beams are directed to an optical laser sheet to form optics module, which illuminates the view of interest in test section. In the present study, the side surface of test section is selected as the view surface, and the upper and bottom parts are selected respectively as the illuminating surfaces for worn cases. The laser pulses are synchronized with a delay generator (BNC Nucleonics) which controlled the lamps and Q-switches, and permits hundreds of nanoseconds time delays between two pulses. The delay generator also triggers and synchronizes the PIV camera double frame to the laser pulses. An Imager sCMOS Camera (La Vision) with 5.5-megapixel double frame mode is used for PIV measurements, and it operates with CamLink frame grabber. The performance of this camera is: inter-frame time < 200 ns, pixel size 6.5 μm × 6.5 μm, maximum resolution 2560 × 2560 pixel at 50 Hz. A fast photodiode (EOS) is used to monitor the actual time delay

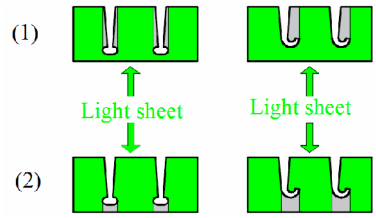

Fig. 10. Schematic diagram of laser projection.

between the light pulses. At a range of pixel resolutions, the cross-correlation algorithm is adopted at each cell in two images to derive the velocity fields. As shown in Fig. 9(b), the local velocity vector of particle can be computed by the particle displacements in time interval Δt. In the present measurements, typical PIV measurement uncertainty of sub-pixel accuracy can be achieved less than 1 % of the main flow speed under test conditions.

For each bending or mushrooming case, it is necessary to carry out two PIV measurements from the bottom and top surfaces, respectively. This is because the light sheet would be blocked by the bending arc or mushroomed part (see the grey areas in Fig. 10). The velocity fields in the whole seal region can be obtained by adding two PIV measurements together.

4. Results and discussion

4.1 Predictions versus measurements

Fig. 11 compares the predicted leakage rates with measurements for the original design, BB1L, FB1L and MR3V cases at a range of pressure ratios. It is observed that, for the original design case, both SST k-ω turbulence model and k-ε turbulence model agree well with the experimental data. However, for the worn cases, only the predictions with SST k-ω turbulence model match well with the experimental data, and the maximum deviations between predictions and measurements are within 3 %. For the k-ε turbulence model, it over-predicts the leakage rates for worn cases by about 10 %. Moreover, compared with the original design case, the leakage rates for bent and mushroomed labyrinth seals are increased, significantly.

Fig. 12 compares the predicted static pressure in each chamber with the experimental data. The locations of pressure probe have already been illustrated in Fig. 7. The open symbols represent the predicted values, and the lines represent the predicted averaged static pressure along axial direction. It is evident that the CFD results match well with the experimental data. The deviation between prediction and measurement is within 2 %. In general, the SST k-ω turbulence model has a high accuracy in predicting the leakage rate, flow structures and also pressure fields in the seal, in contrast to the k-ε turbulence model.

Fig. 13 compares the predicted meridian flow fields with PIV measurements for the original design case. It is seen that there is a large scale of vortex formed in each chamber. Note

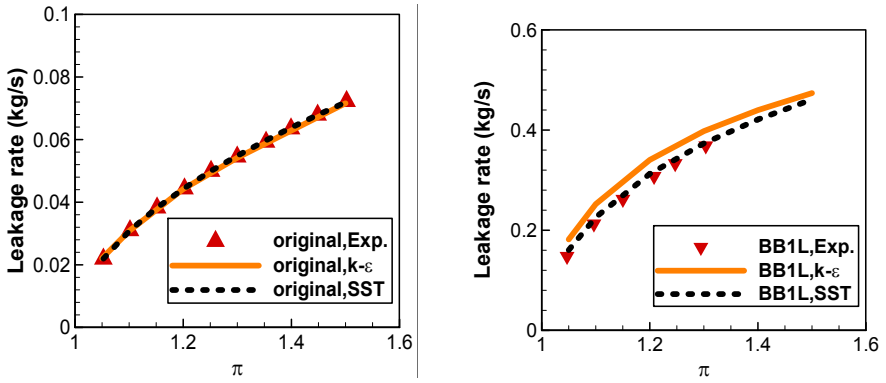

(a) Design case (*Re* range = 3600-12000)

(b) BB1L (*Re* = 24000-62000)

(c) FB1L (*Re* = 27000-78000)

(d) MR3V (*Re* = 32000-91000)

Fig. 11. Comparisons of predictions and measurements for leakage rates.

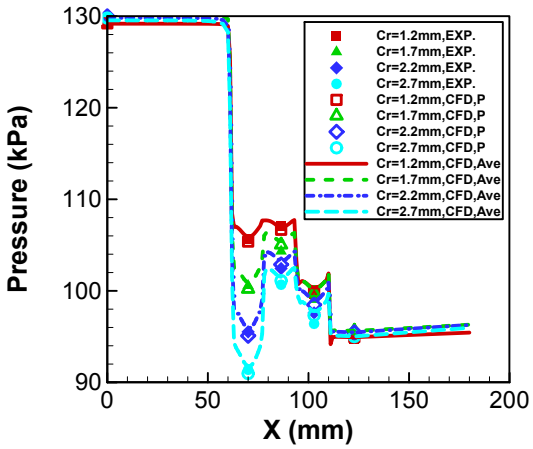

Fig. 12. Comparisons of predictions and measurements for staic pressures in seal chambers (design case, π = 1.35).

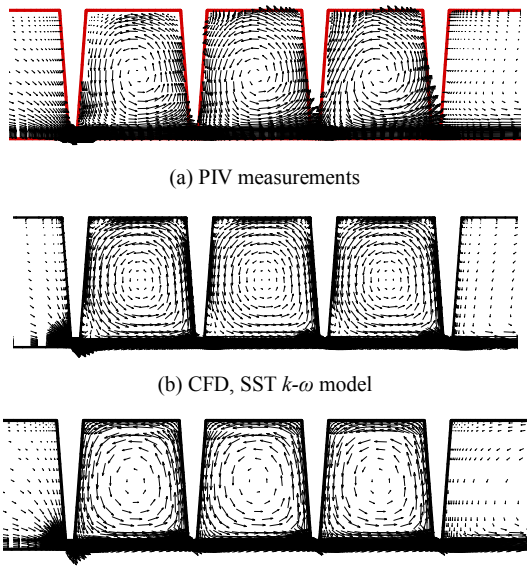

(a) PIV measurements

(b) CFD, SST *k*-*ω* model

(c) CFD, *k*-*ε* model

Fig. 13. Velocity fields in labyrinth seal for original design case (π = 1.1, *Re* = 5200).

that the predicted velocity vectors match well with the experimental data. In addition, for the design case, the predicted flow fields are similar for SST *k*-*ω* turbulence model and *k*-*ε* turbulence model.

Fig. 14 illustrates the flow fields in the backward bending case. It is observed that there are two vortices located near the bending arc (label A and B in Fig. 14(a)). The small vortex downstream the fin tip (label B in Fig. 14(a)) is generated due to flow separation and reattachment, which have pronounced influence on the impingement angle of leakage jet near clearance gap.

Fig. 15 compares the predicted flow fields in the forward bending case with PIV measurements. Unlike the backward bending case, two counter-rotating vortices are formed in each chamber for forward bending case. This flow pattern enhances

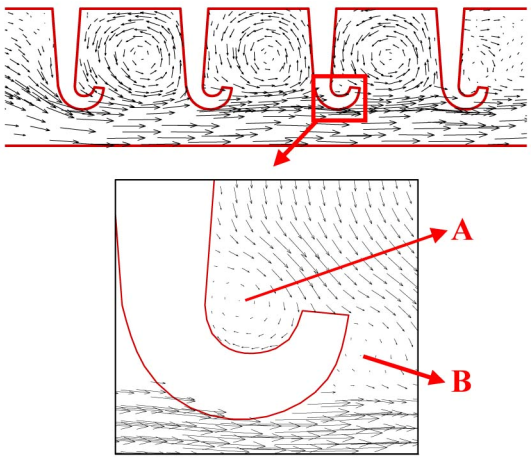

(a) PIV measurements

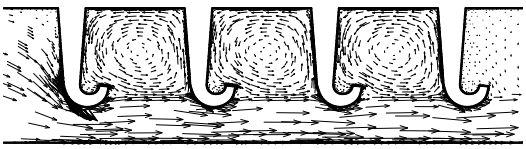

(b) CFD, SST k-ω model

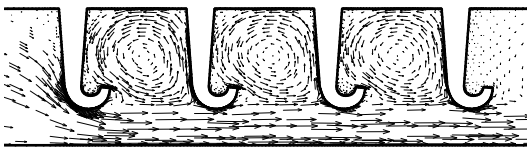

(c) CFD, k-ε model

Fig. 14. Velocity fields in labyrinth seal for BB1L case (π = 1.05, Re = 24000).

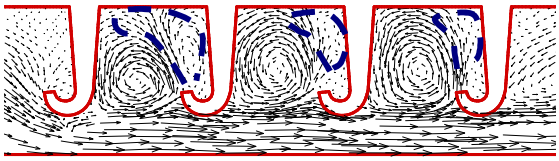

(a) PIV measurements

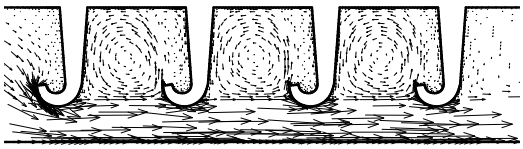

(b) CFD, SST k-ω model

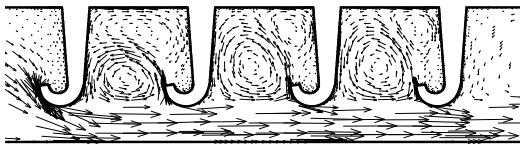

(c) CFD, k-ε model

Fig. 15. Velocity fields in labyrinth seal for FB1L case (π = 1.05, Re = 27000).

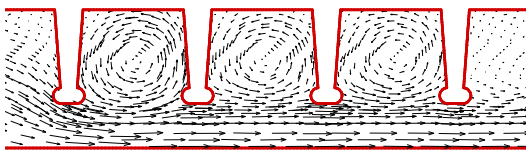

(a) PIV measurements

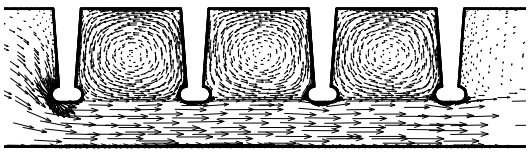

(b) CFD, SST k-ω model

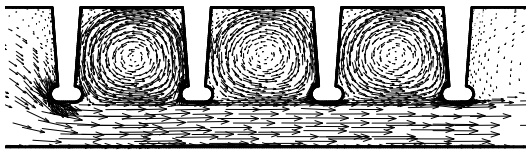

(c) CFD, k-ε model

Fig. 16. Velocity fields in labyrinth seal for MR3V case (π = 1.05, Re = 32000).

the kinetic energy dissipations in the chamber in contrast to the backward bending case. Compared with the PIV measurements, the SST k-ω turbulence model exhibits higher accuracy in predicting the flow fields than that of k-ε turbulence model, especially in the first chamber.

Fig. 16 shows the meridian flow fields in the mushroomed case. The flow patterns in each chamber are quite similar to the design case. Due to the round tips, the streamlines near the fin tip is slightly curved, especially in the first chamber.

From the above discussion, it indicates that the SST k-ω turbulence model has a higher accuracy in predicting the leakage rate and flow patterns in the labyrinth seal, especially for the worn cases. Therefore, the SST k-ω turbulence model is finally adopted to analyze the effect of bending and mushrooming damages on leakage performance of labyrinth seals.

4.2 Effect of bending and mushrooming on leakage

Fig. 17 plots the leakage ratios ξ for the backward bending and forward bending cases at two pressure ratios. It is seen that, for all cases, ξ is almost linearly increased with the increase of effective clearance (c_r^*). With the same effective clearance (c_r*) and the unbent height (U), the forward bending with small unbent height (see FB2 and BB2, FB3 and BB3 in Fig. 17) has lower leakage ratio ξ than that of backward bending case. However, with large unbent height (see FB1 and BB1 in Fig. 17), the leakage ratios ξ for forward bending and backward bending cases are almost the same in large clearance c_r* cases. Therefore, labyrinth fin with larger flexibility has less degradation of leakage performance in rubbing events. Another observation is that, for the forward bending case, FB2 almost has the identical leakage ratio ξ with FB3. This indi-

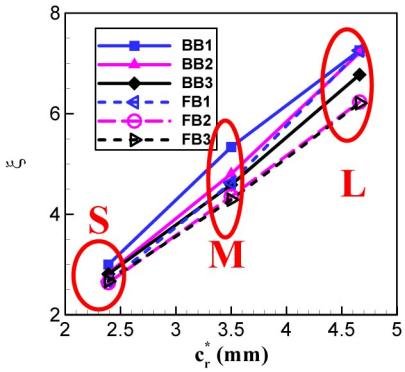

(a) $\pi = 1.1$

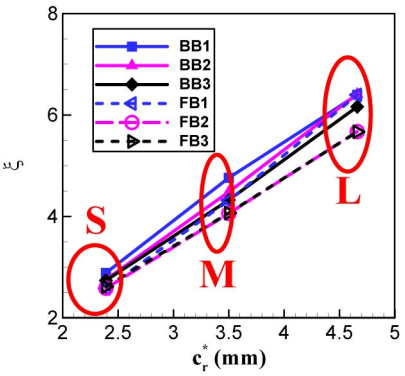

(b) $\pi = 1.5$

Fig. 17. Leakage ratio versus effective clearance for bending cases.

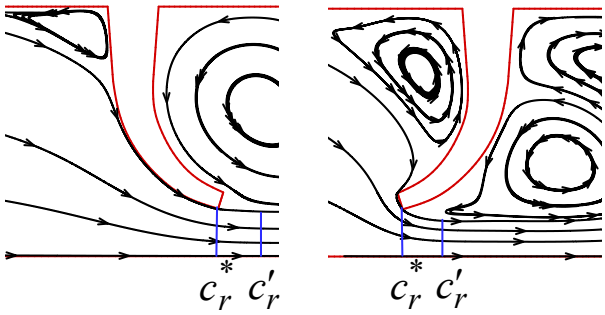

(a) BB2M (Re = 25000) (b) FB2M (Re = 23000)

Fig. 18. Streamlines near the first clearance for bending cases (π = 1.1).

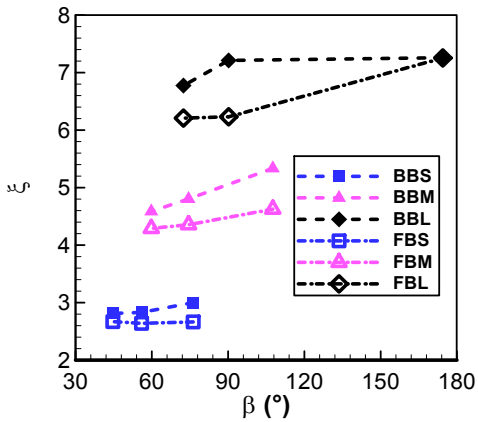

(a) π = 1.1

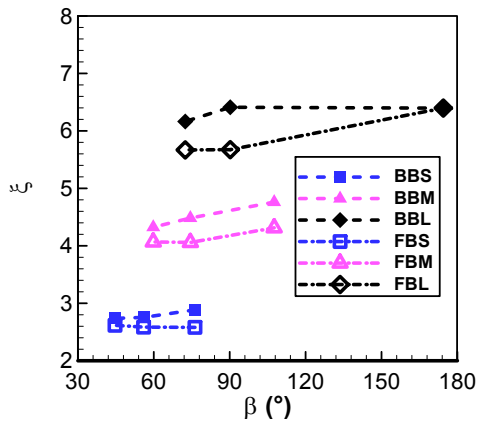

(b) π = 1.5

Fig. 19. Leakage ratio versus bending angle for the bending cases.

cates the unbent height would have little effect on the leakage ratio if it decreases to a certain value (in this study, U < 5.27 mm) for the forward bending damage.

Fig. 18 illustrates the streamlines near the first clearance gap in the backward bending case (BB2M) and the forward bending case (FB2M) with the same effective clearance (c_r^*) and unbent height (U). It is seen that the FB2M case has a stronger vena-contracta effect than that of BB2M case (see c_r' in Fig. 18). The stronger vena-contracta effect will lead to a smaller discharge clearance and larger chamber vortices, which enlarge the kinetic energy dissipation in the chamber for the leakage flow. This is why the forward beading case has a lower leakage rate than that of backward bending case with the same effective clearance and unbent height (see Fig. 17).

Fig. 19 plots the relations between leakage ratio ξ and bending angle β for bending cases. Similar with Fig. 17, the forward bending case has a lower leakage ratio ξ than that of backward bending case with the same bending angle. It is also seen that ξ is increased with the increase of β except the large backward bending case (BB3L). However, as β is increased close to 180 degrees, ξ for forward bending case is almost equal to that of backward bending case. These trends can be explained by Fig. 20, which shows the flow fields near the first clearance gaps for the bending cases (BB1L, BB2L, BB3L, FB1L, FB2L and FB3L) with the same effective clearance c_r^*. It is clearly seen that the discharge clearances (c_r') for backward bending and forward bending are very close as β is close to 180 degree (Fig. 20(a)). However, as β decreases, the discharge clearance (c_r') for the forward bending case is much smaller than the backward bending case. As a result, the leakage ratio for the forward bending case is much lower than the backward bending case. Another observation is that the effective clearance c_r^* is almost equal to the discharge clearance (c_r') for the backward bending cases. However, for the forward bending cases, the discharge clearances (c_r') are smaller than

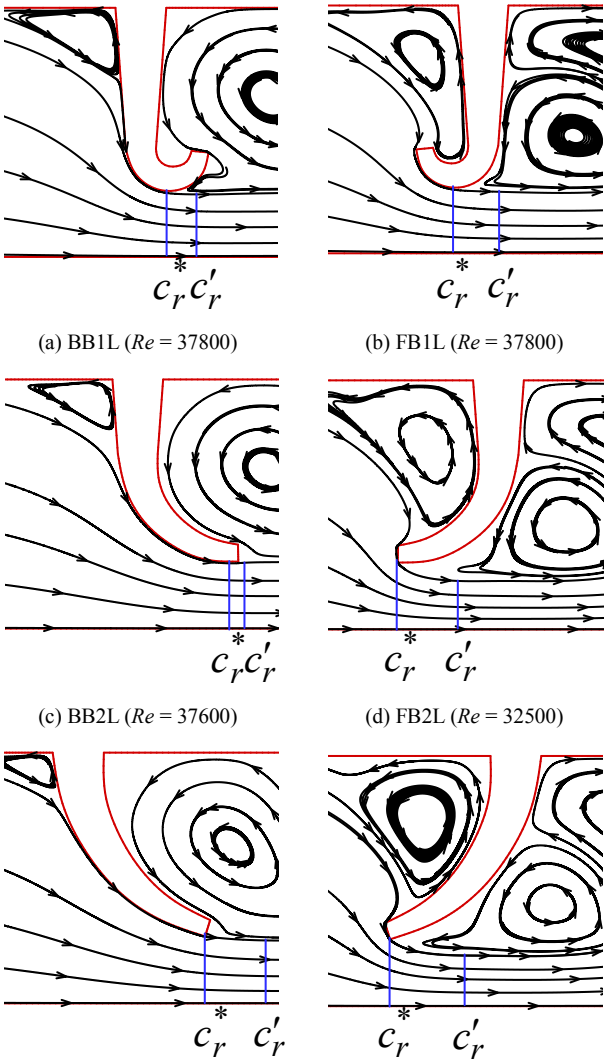

(a) BB1L (*Re* = 37800) (b) FB1L (*Re* = 37800)

(c) BB2L (*Re* = 37600) (d) FB2L (*Re* = 32500)

(e) BB3L (*Re* = 35300) (f) FB3L (*Re* = 32300)

Fig. 20. Streamlines near the first clearance for bending cases with same effective.

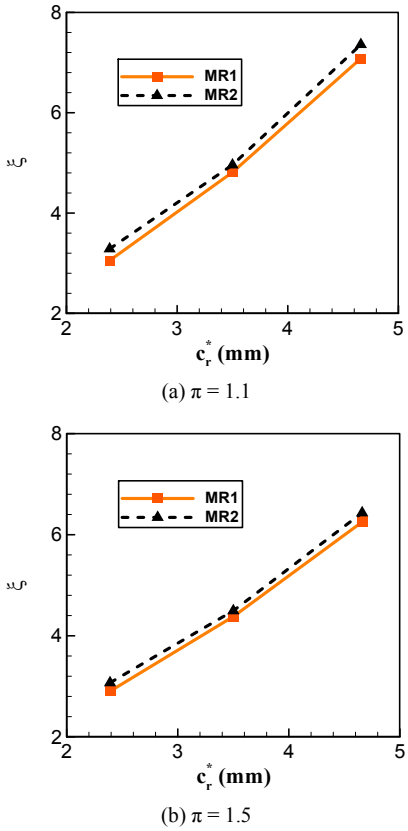

(a) π = 1.1

(b) π = 1.5

Fig. 21. Leakage ratio versus effective clearance for the mushrooming cases.

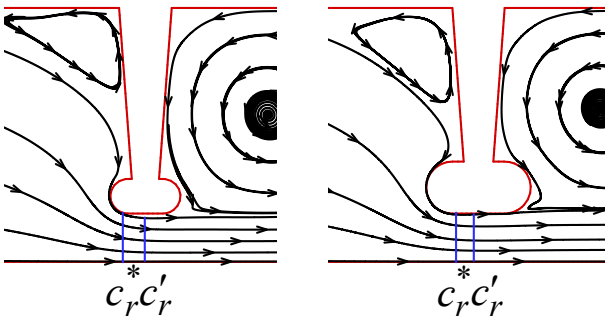

(a) MR1M (*Re* = 25100) (b) MR2M (*Re* = 25800)

Fig. 22. Streamlines near the first clearance for the mushrooming case with same effective clearances (c_r* = 3.50 mm, π = 1.1).

the effective clearance c_r^*. In general, for the bending cases, the discharge behaviors, including the leakage rate and flow patterns, are quite sensitive to the effective clearance and bending geometries which affect the discharge clearance significantly near the gap.

Fig. 21 shows the leakage ratios ξ versus effective clearance c_r* for mushrooming cases at two pressure ratios. Similar with the bending cases, ξ is almost linearly increased with the increase of c_r*. However, as the mushrooming radius *Rm* increases, ξ is increased slightly. It is observed that ξ is increased by about 4 % as *Rm* increases from 1.2 mm to 1.8 mm.

This can also be explained by the flow patterns in the labyrinth seal, as shown in Fig. 22. It is seen that the labyrinth fin with a smaller mushrooming radius *Rm* is more likely to produce flow separation, which leads to a stronger vena-contracta effect. Therefore, the discharge clearance for the MR2M case is slightly larger than that of MR1M case, and also the vortices in seal chamber for the MR2M case are slightly larger than that of MR1M case.

Fig. 23 plots the leakage ratios ξ versus pressure ratio π for the worn cases. It is seen that, for the bending cases, ξ is slightly increased from π = 1.05 to 1.1, and then decreased with the increase of π. For the mushrooming cases with small clearances (MR1S and MR2S), ξ is slightly increased from π = 1.05 to 1.1, and then decreased with the increase of π. However, for the mushrooming cases with large clearances (MR1M, MR1L, MR2M and MR2L), ξ is decreased from π =

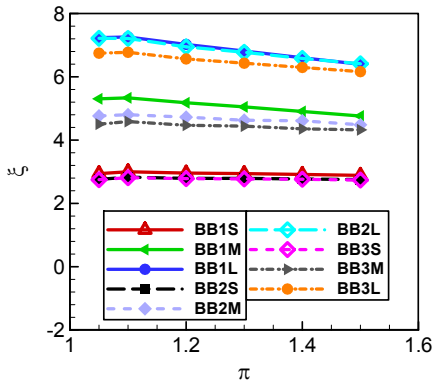

(a) Backward bending

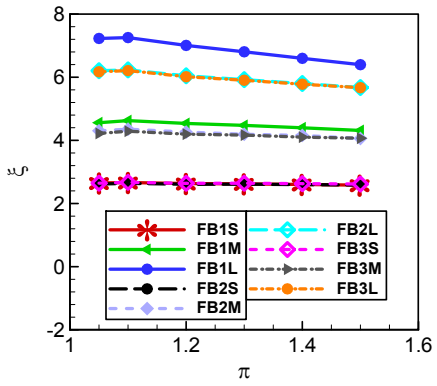

(b) Forward bending

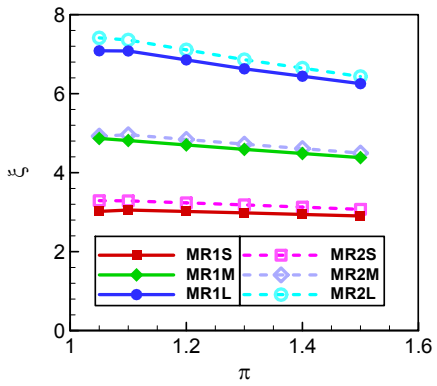

(c) Mushrooming

Fig. 23. Leakage ratio versus pressure ratio for worn cases.

1.05 to 1.5. This indicates the vena-contracta effect is enhanced with the increase of π, which has a very important effect on the leakage performance of mushroomed labyrinth seal.

In general, the leakage ratio is varied slightly with the pressure ratio, especially in the small bending and mushrooming cases. For the bending cases, the leakage ratio is sensitive to the bending angle and unbent height. For the mushrooming cases, however, it changes slightly with the mushrooming radius. After rub, the leakage degradation of straight-through labyrinth seal in backward bending case and mushrooming case are more serious than that in forward bending case.

5. Conclusions

In this paper, the effects of teeth bending (forward bending and backward bending) and mushrooming on leakage performance of a straight-through labyrinth seal are investigated with experimental tests and numerical simulations. The major findings are as follows:

(1) For the original design case, the predicted leakage rates with *k-ε* and SST *k-ω* turbulence models are almost identical. The predictions agree well with the experimental data. However, in the bent and mushrooming cases, the *k-ε* turbulence model over-predicts the leakage rate by about 10 %, while the difference between predicted leakage rate and measurement is within 3 % for SST *k-ω* turbulence model. For the flow fields, *k-ε* and SST *k-ω* turbulence models almost have the same accuracy in resolving the vortex system for the original design cases. However, in the bent case with large separations in seal chambers, the SST *k-ω* turbulence model has a higher accuracy in resolving the counter-rotating vortices than the *k-ε* turbulence model.

(2) For the mushrooming case, the discharge behavior is mainly determined by the effective clearance and slightly affected by the mushroom radius. As the mushroom radius increases from 1.2 mm to 1.8 mm, the leakage ratio is only increased by about 4 %.

(3) For the bending case, the discharge behavior is mainly affected by the effective clearance and bending geometries (bending angle) at the fixed pressure ratio. The leakage ratios for the forward bending cases are smaller than those for the backward bending case due to decreased discharge clearances. As the bending angle is close to 180 degrees, the leakage ratio of forward bending case is almost equal to that of backward bending case. As the unbent height *U* decreases to a certain value, it will have little influence on the leakage ratio for the forward bending damage labyrinth seal. However, labyrinth fin with larger flexibility will mitigate the leakage degradation of straight-through labyrinth seal in rubbing events.

(4) For bending and mushrooming cases, the leakage ratio is slightly decreased with the increase of pressure ratio except in small pressure ratio condition (around 1.05-1.1).

Acknowledgments

The authors are grateful for the supports by National Natural Science Foundation of China (Grant No. 51576151) and Natural Science Foundation of Shaanxi Province (Grant No. 2018JQ5027).

Nomenclature

B : Width of test section [mm]
c_r : Clearance in design case [mm]
Hs : Tooth height [mm]
Ls : Pitch [mm]
P : Pressure [Pa]
Rb : Bent radius [mm]

Re : Reynolds number
Rm : Mushroom radius [mm]
Sm : Distance between two mushroom arcs [mm]
T : Temperature [K]
U : Unbent height [mm]
W : Thickness of tooth tip [mm]
Wr : Thickness of tooth root [mm]

Greek symbols

α : Tooth angle [°]
β : Bent angle [°]
μ : Fluid dynamic viscosity coefficient[Pa·s]
π : Pressure ratio [-]
ρ : Fluid density[kg/m^3]
ξ : Leakage ratio [-]

Superscripts

* : Effective value
’ : Discharge value

Subscripts

0 : Inlet condition
1 : Outlet condition

Abbreviations

BB : Backward bending
FB : Forward bending
L : Large rub
M : Medium rub
MR : Mushrooming
SST : Shear stress transport
S : Small rub
V : Validation by experiment

References

[1] R. E. Chupp, R. C. Hendricks, S. B. Lattime and B. M. Steinetz, Sealing in turbomachinery, *Journal of Propulsion and Power*, 22 (2) (2006) 313-349.

[2] M. L. Adams, *Rotating machinery vibration: From analysis to troubleshooting,* Second Ed. CRC Press Inc, Florida, USA (2009).

[3] J. Vance, F. Zeidan and B. Murphy, *Machinery vibration and rotordynamics*, Wiley, New Jersey, USA (2010).

[4] F. Ghasripoor, N. A. Turnquist, M. Kowalczyk and B. Couture, Wear prediction of strip seals through conductance, *ASME Paper No. GT 2004-53297.*

[5] J. M. Xu, Effects of operating damage of labyrinth seal on seal leakage and wheelspace hot gas ingress, *Ph.D. Thesis*, Texas A & M University, College Station, Texas, USA (2006).

[6] N. Herrmann, K. Dullenkopf and H. J. Bauer, Flexible seal strip design for advanced labyrinth seals in turbines, *ASME Paper No. GT2013-95424.*

[7] X. Yan, L. J. Lei, J. Li and Z. P. Feng, Effect of bending and mushrooming damages on heat transfer characteristic in labyrinth seals, *ASME Journal of Engineering for Gas Turbines and Power,* 136 (4) (2014) 041901.

[8] Z. S. Liu, X. W. Wang and W. Dou, Using acoustic emission and vibration detection to identify the rotor-stator rubbing, *ASME Paper No. DETC2007-34303.*

[9] S. Wittig, K. Jacobsen, U. Schelling and S. Kim, Heat transfer in stepped labyrinth seals, *Journal of Engineering for Gas Turbines & Power*, 110 (1) (1988) 63-69.

[10] V. Schramm, K. Willenborg, S. Kim and S. Wittig, Influence of a honeycomb facing on the flow through a stepped labyrinth seal, *ASME Journal of Engineering for Gas Turbines and Power*, 124 (1) (2002) 140-146.

[11] R. Paolillo, C. Z. Wang, T. K. Vashist, D. Cloud, F. M. G. Bingen and G. A. Kool, Rotating seal rig experiments: test results and analysis modeling, *ASME Paper No. GT2006-90957.*

[12] M. Micio, B. Facchini, L. Innocenti and F. Simonetti, Experimental investigation on leakage loss and heat transfer in a straight through labyrinth seal, *ASME Paper No. GT2011-46402.*

[13] J. K. Whalen, E. Alvarez and L. P. Palliser, Thermoplastic labyrinth seals for centrifugal compressors, *Proceedings of the Thirty-Third Turbomachinery Symposium* (2004) 113-126.

[14] T. Pychynski, K. Dullenkopf and H. J. Bauer, Theoretical study on the origin of radial cracks in labyrinth seal fins due to rubbing, *ASME Paper No. GT2013-94834.*

[15] Y. Dogu, M. C. Sertcakan, K. Gezer, M. Kocagül, E. Arıcan and M. S. Ozmusul, Labyrinth seal leakage degradation due to various types of wear, *ASME Journal of Engineering for Gas Turbines and Power*, 139 (6) (2017) 062504.

[16] H. H. Chougule, D. Ramerth, D. Ramchandran and D. Kandala, Numerical investigation of worn labyrinth seals, *ASME Paper No. GT2006-90690.*

[17] D. Collins, J. Teixeira and P. Crudgington, The degradation of abradable honeycomb labyrinth seal performance due to wear, *Sealing Technology*, 8 (2008) 7-10.

[18] T. Pychynski, C. Höfler and H. J. Bauer, Experimental study on the friction contact between a labyrinth seal fin and a honeycomb stator, *ASME Paper No. GT2015-42430.*

[19] W. Waschka, S. Wittig and S. Kim, Influence of high rotational speeds on the heat transfer and discharge coefficients in labyrinth seals, *Journal of Turbomachinery*, 114 (2) (1990) 462-468.

[20] W. Waschka, S. Wittig, S. Kim and T. Scherer, Heat transfer and leakage in high-speed rotating stepped labyrinth seals, *AGARD, Heat Transfer and Cooling in Gas Turbines* (1993) N93-29926 11-07.

[21] ANSYS, *ANSYS CFX-Solver Theory Guide: Version 11.0,* ANSYS, Canonsburg, PA (2007).

Xin Yan is a Professor at Institute of Turbomachinery, Xi'an Jiaotong University. His main research interest has been in Computational Fluid Dynamics with emphasis in turbomachinery aerodynamics and heat transfer. He is also involved in experimental work to understand complex flow physics.

Xinbo Dai is a Ph.D. candidate at Institute of Turbomachinery, Xi'an Jiaotong University, China. His research interests include advanced sealing technology and thermal-fluid-solid interactions.